Proceedings of DETC'01
ASME 2001 Design Engineering Technical Conference
and Computers and Information in Engineering Conference
Pittsburgh, PA, September 9-12, 2001

DETC2001/VIB-21608

NONLINEAR DYNAMICS OF THE WOODPECKER TOY

Remco I. Leine[a*] **Christoph Glocker**[b] **Dick H. van Campen**[a]

[a] Department of Mechanical Engineering
Eindhoven University of Technology
P. O. Box 513, 5600 MB Eindhoven
The Netherlands
Email: r.i.leine@tue.nl

[b] Institute of Mechanical Systems
Center of Mechanics, ETH Zentrum
CH-8092 Zürich
Switzerland
Email: christoph.glocker@imes.mavt.ethz.ch

ABSTRACT

This paper studies bifurcations in systems with impact and friction, modeled with a rigid multibody approach. Knowledge from the field of Nonlinear Dynamics is therefore combined with theory from the field of Nonsmooth Mechanics. The nonlinear dynamics is studied of a commercial wooden toy. The toy shows complex dynamical behaviour but can be studied with a one-dimensional map, which allows for a thorough analysis of the bifurcations.

INTRODUCTION

Impact with friction can be present between two or more bodies of a system. Periodic impact of colliding bodies or rubbing of bodies in contact can be highly detrimental to mechanical systems, like rattling in gear boxes and stick-slip phenomena in cutting processes. On the other hand, many mechanical systems rely on impulsive and stick-slip processes to perform their intended functions (a hammer drill for instance). Modeling of systems with impact and friction receives increasingly more attention in literature, due to the need to predict, control or avoid vibrations in systems with impact and friction. The global dynamics of the system is therefore of interest, and not the tribological processes of the contact surface, which allows for simplified contact models.

A rigorous way to deal with systems with impact and friction is the rigid multibody approach [Brogliato, 1999, Glocker, 1995, Pfeiffer and Glocker, 1996]. This approach models the system as a set of rigid bodies, interconnected by joints, springs, dashpots and nonlinear couplings. Wave effects are neglected in the rigid body approach. Impact between the bodies and stick-slip transitions of bodies in contact are considered to be instantaneous and are described by contact laws. Newton's impact law or Poisson's law are usually taken as impact law in normal direction. Newton's law relates post-impact velocities to pre-impact velocities with a restitution coefficient. Poisson's law treats the impact as a compression and expansion phase and relates the impulse stored during compression to the impulse released in the expansion phase with a restitution coefficient. Amontons-Coulomb's law, in which the friction force is in the opposite direction of the relative velocity and proportional to the normal force, is usually taken as contact law in tangential direction. The restitution coefficient and friction coefficient can be measured in a straightforward manner from simple experiments [Beitelschmidt, 1999]. The rigid body approach avoids stiff differential equations and is therefore more economical than regularization methods. This advantage is at the cost of a more complex mathematical formulation. Multibody systems with multiple contacts bring forth a combinatorial problem of large dimensions. If the state in one contact changes, for example from contact to detachment or from stick to slip, all other contacts are also influenced, which makes a search for a new set of contact configurations necessary. A standard way to perform the search for a new contact configuration is to formulate the problem as a Linear Complementarity Problem, for which standard numerical solvers are available. If the transition times of impact and stick-slip transitions are small in comparison with the times between transitions, and if wave effects can be neglected, then the rigid

*Address all correspondence to this author.

body approach can be expected to give good results.

As a second analysis step, one might not only be interested in time integration, but also in studying stable and unstable equilibria and periodic solutions and their dependencies on parameters of the system. Nonlinear analysis methods, such as shooting and path-following techniques, have been developed in the field of Nonlinear Dynamics, to find periodic solutions and to follow branches of periodic solutions for varying system parameters. A branch of periodic solutions can fold or bifurcate at critical values of the system parameter. This qualitative change is called 'bifurcation'. Bifurcations are essential for understanding why vibrations are created, disappear or change qualitatively when a design variable of the system is varied. The theory of bifurcations is therefore important for the analysis of the dynamical behaviour and design of systems.

Unilateral contact laws, as are used in the rigid body approach, lead to nonsmooth mathematical models with discontinuities in the generalized velocities due to impacts. Bifurcations in smooth systems are well understood [Guckerheimer and Holmes, 1983] but little is known about bifurcations in nonsmooth systems [Leine, 2000]. Literature on bifurcations in nonsmooth mechanical systems seems to be divided in two groups:

1. Bifurcations in systems with *friction*, which belong to the class of Filippov-systems. Literature on this topic is vast (for instance [Dankowicz and Normark, 2000, Galvanetto and Knudsen, 1997, Leine and van Campen, 1999), Leine and van Campen, 2000, Popp *et al.*, 1995, Van de Vrande *et al.*, 1999, Wiercigroch, 1996, Yoshitake,and Sueoka, 2000]). A general theory for bifurcations in Filippov-systems is not available but attempts to explore in that direction are made [di Bernardo *et al.*, 1999, Leine *et al.*, 2000, Leine, 2000].
2. Bifurcations in systems with *impact* [Foale and Bishop, 1994, Ivanov, 1996, Meijaard, 1996, Nordmark, 1997, Peterka, 1996]. The impacts are almost always considered to be frictionless.

Literature on bifurcations in systems with combined friction and impact is hardly available. An impact oscillator with friction is studied in [Blazejczyk-Okolewska and Kapitaniak, 1996] but the impact and friction are in different contact points for this system and the contact problem is therefore decoupled.

The present paper studies bifurcations in a geometrically simple dynamical system with impact and friction occurring in the same contact. The system is a mechanical wooden toy, which shows limit cycling behaviour, and can very well be modeled with the rigid body approach. Although the toy might look simple at first sight, its dynamics is rather complicated and governed by non-standard bifurcations.

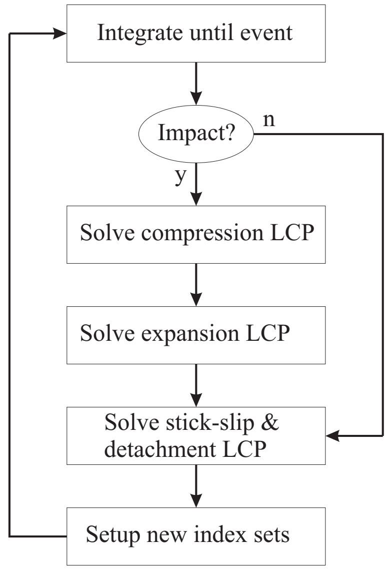

Figure 1. Flowchart of the algorithm.

MATHEMATICAL MODELING OF IMPACT WITH FRICTION

The dynamics of a constrained multibody system can be expressed by the equation of motion

$$\mathbf{M}(t,\mathbf{q})\ddot{\mathbf{q}} - \mathbf{h}(t,\mathbf{q},\dot{\mathbf{q}}) - \sum_{i\in I_S}(\mathbf{w}_N\lambda_N + \mathbf{w}_T\lambda_T)_i = \mathbf{0}, \qquad (1)$$

where $\mathbf{M}$ is the symmetric mass matrix, $\mathbf{q}$ the vector with generalized coordinates, $\mathbf{h}$ the vector with all smooth elastic, gyroscopic and dissipating generalized forces and $\boldsymbol{\lambda}_N$ and $\boldsymbol{\lambda}_T$ the vectors with normal and tangential contact forces. The time-variant set I_S contains the n_S indices of the potentially active constraints. The constraints are specified by the normal contact distances g_{Ni} and the tangential relative velocity $\dot{g}_{Ti}$ of contact point i. The contact velocities and accelerations in normal and tangential direction can be expressed in the generalized velocities

$$\begin{bmatrix}\dot{\mathbf{g}}_N\\ \dot{\mathbf{g}}_T\end{bmatrix} = \begin{bmatrix}\mathbf{W}_N\\ \mathbf{W}_T\end{bmatrix}\dot{\mathbf{q}} + \begin{bmatrix}\hat{\mathbf{w}}_N\\ \hat{\mathbf{w}}_T\end{bmatrix} \qquad \in \mathbb{R}^{2n_S}, \qquad (2)$$

$$\begin{bmatrix}\ddot{\mathbf{g}}_N\\ \ddot{\mathbf{g}}_T\end{bmatrix} = \begin{bmatrix}\mathbf{W}_N\\ \mathbf{W}_T\end{bmatrix}\ddot{\mathbf{q}} + \begin{bmatrix}\bar{\mathbf{w}}_N\\ \bar{\mathbf{w}}_T\end{bmatrix} \qquad \in \mathbb{R}^{2n_S}. \qquad (3)$$

A mathematical theory for the dynamics of rigid bodies with Poisson-Coulomb impact is formulated in [Glocker, 1995,

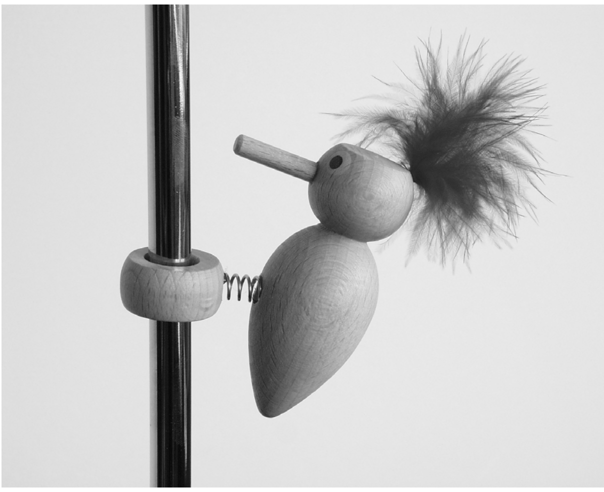

Figure 2. The Woodpecker Toy.

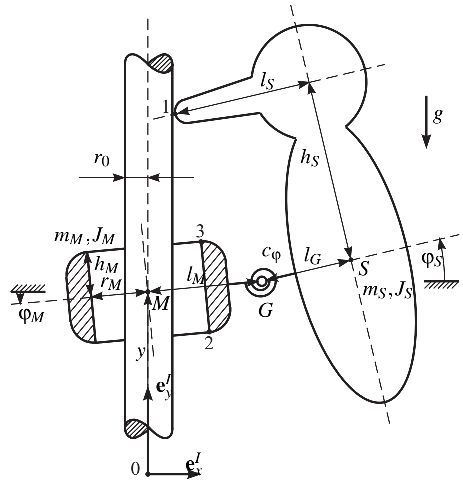

Figure 3. Model of the Woodpecker Toy (not on scale).

Glocker, 2000, Pfeiffer and Glocker, 1996]. The contact problem for stick-slip transitions, detachment and impact are formulated in [Glocker, 1995, Pfeiffer and Glocker, 1996] as a Linear Complementarity Problems. A linear complementarity problem (LCP) [Cottle and Dantzig, 1968] is a set of linear equations

$$\mathbf{y} = \mathbf{A}\mathbf{x} + \mathbf{b} \tag{4}$$

subjected to the complementarity conditions

$$\mathbf{y} \geq \mathbf{0}, \qquad \mathbf{x} \geq \mathbf{0}, \qquad \mathbf{y}^{\mathrm{T}}\mathbf{x} = 0, \tag{5}$$

for which the vectors $\mathbf{x}$ and $\mathbf{y}$ have to be solved for given $\mathbf{A}$ and $\mathbf{b}$. The impact law of Poisson is applied, consisting of an compression phase during which impulse is stored and an expansion phase during which part of the stored impulse is released. Coulomb's friction law is applied for the tangential constraint.

Figure 1 shows how the order of the different phases in the integration procedure. The equation of motion for given index sets is numerically integrated until an impact, stick-slip or detachment event occurs. If the event is an impact event, the LCP's for compression and expansion have to be solved, after which the new generalized velocities $\dot{\mathbf{q}}$ are known. Subsequently, a LCP on acceleration level has to be solved, because the impact might cause stick-slip transitions or detachment of other contacts. The new accelerations $\ddot{\mathbf{q}}$ are known after having solved all necessary LCP's. The new index sets can then be setup and a new integration phase can start.

THE WOODPECKER TOY

A Woodpecker Toy (Figure 2) hammering down a pole is a typical system with limit cycles combining impacts, friction and jamming. The toy consists of a sleeve, a spring and the woodpecker. The hole in the sleeve is slightly larger than the diameter of the pole, thus allowing a kind of pitching motion interrupted by impacts with friction.

The scientific study of this toy dates back to [Pfeiffer, 1984]. At that time one was not able to deal with systems with impact and friction. A heuristic model was presented in [Pfeiffer, 1984], in which the friction losses were determined experimentally. The lack of a more general theory gave the onset for the work in [Glocker, 1995, Pfeiffer and Glocker, 1996], in which a mathematical theory for impact problems with friction is formulated. In [Glocker, 1995, Pfeiffer and Glocker, 1996] a model for the Woodpecker Toy was presented as example for the developed theory. In this section a bifurcation analysis will be given of the model presented in [Glocker, 1995, Pfeiffer and Glocker, 1996], with the aid of a one-dimensional mapping. First the model will be briefly given.

The Woodpecker Toy is a system which can only operate in the presence of friction as it relies on combined impacts and jamming. Restitution of the beak with the pole is not essential for a periodic motion but enlarges the resemblance with the typical behaviour of a woodpecker. The motion of the toy lies in a plane, which reduces the number of degrees of freedom to model the system.

The system (Figure 3) possesses three degrees of freedom $\mathbf{q} = \left[y \ \varphi_M \ \varphi_S\right]^{\mathrm{T}}$, where φ_S and φ_M are the absolute angles of rotation of the woodpecker and the sleeve, respectively, and y describes the vertical displacement of the sleeve. Horizontal displacement of the sleeve are negligible. Due to the clearance between sleeve and pole, the lower or upper edge of the sleeve may come into contact with the pole, which is modeled by constraints 2 and 3. Furthermore, contact between the beak of the woodpecker with the pole is expressed by constraint 1. The special geometry of the design enables us to assume only small deviations of the rotations. Thus a linearized evaluation of the system's kinematics is sufficient and leads to the model listed below. The mass matrix **M**, the force vector **h** and the constraint vectors **w** follow from Figure 3 in a straightforward manner. They are

$$\mathbf{M} = \begin{bmatrix} (m_S + m_M) & m_S l_M & m_S l_G \\ m_S l_M & (J_S + m_S l_M^2) & m_S l_M l_G \\ m_S l_G & m_S l_M l_G & (J_S + m_S l_G^2) \end{bmatrix} \tag{6}$$

$$\mathbf{h} = \begin{bmatrix} -(m_S + m_M) \\ -c_\varphi(\varphi_M - \varphi_S) - m_S g l_M \\ -c_\varphi(\varphi_S - \varphi_M) - m_S g l_G \end{bmatrix} \tag{7}$$

$$\begin{aligned} g_{N1} &= (l_M + l_G - l_S - r_0) - h_S \varphi_S \\ g_{N2} &= (r_M - r_0) + h_M \varphi_M \\ g_{N3} &= (r_M - r_0) - h_M \varphi_M \end{aligned} \tag{8}$$

$$\mathbf{w}_{N1} = \begin{bmatrix} 0 \\ 0 \\ -h_S \end{bmatrix}, \quad \mathbf{w}_{N2} = \begin{bmatrix} 0 \\ h_M \\ 0 \end{bmatrix}, \quad \mathbf{w}_{N3} = \begin{bmatrix} 0 \\ -h_M \\ 0 \end{bmatrix} \tag{9}$$

$$\mathbf{w}_{T1} = \begin{bmatrix} 1 \\ l_M \\ l_G - l_S \end{bmatrix}, \quad \mathbf{w}_{T2} = \begin{bmatrix} 1 \\ r_M \\ 0 \end{bmatrix}, \quad \mathbf{w}_{T3} = \begin{bmatrix} 1 \\ r_M \\ 0 \end{bmatrix} \tag{10}$$

$$\bar{\mathbf{w}}_N = \hat{\mathbf{w}}_N = \bar{\mathbf{w}}_T = \hat{\mathbf{w}}_T = \mathbf{0}. \tag{11}$$

Results

We consider for the numerical analysis of the Woodpecker Toy the same data set as taken in [Glocker, 1995, Pfeiffer and Glocker, 1996]:

Dynamics: $m_M = 0.0003$ kg; $J_M = 5.0\ 10^{-9}$ kg m^2;
$m_S = 0.0045$ kg; $J_S = 7.0\ 10^{-7}$ kg m^2; $g = 9.81$ m/s^2;
Geometry: $r_0 = 0.0025$ m; $r_M = 0.0031$ m;
$h_M = 0.0058$ m; $l_M = 0.010$ m; $l_G = 0.015$ m;
$h_S = 0.020$ m; $l_S = 0.0201$ m;
Contact: $\mu_1 = \mu_2 = \mu_3 = 0.3$; $\varepsilon_{N1} = 0.5$; $\varepsilon_{N2} = \varepsilon_{N3} = 0.0$;

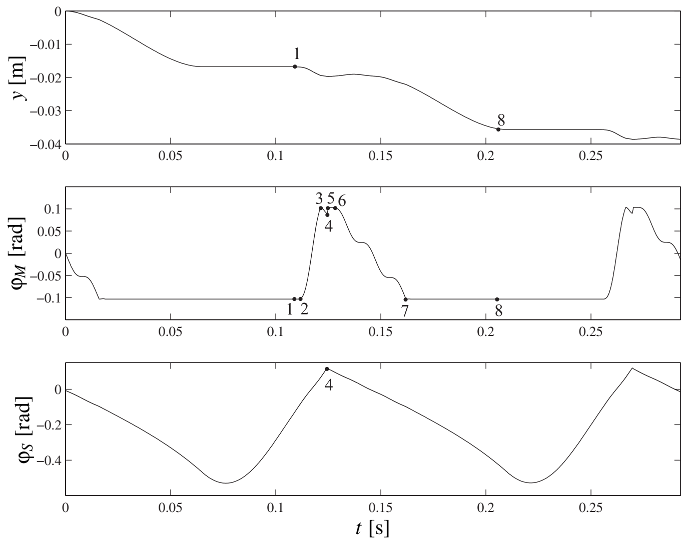

Figure 4. Time history of the coordinates.

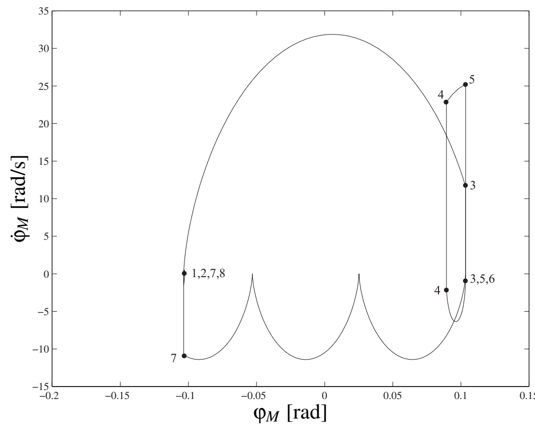

Figure 5. Phase space portraits.

The motion of the sleeve and woodpecker are limited by the contacts, $|\varphi_M| \leq (r_M - r_0)/h_M = 0.1034$ rad and $\varphi_S \leq (l_M + l_G - l_S - r_0)/h_S = 0.12$ rad. The system has a (marginally stable) equilibrium position, in which the woodpecker is hanging backward on the jamming sleeve, $\mathbf{q} = \begin{bmatrix} y & -0.1034 & -0.2216 \end{bmatrix}^{\mathrm{T}}$. The jamming of the sleeve with the pole at that position is only possible if $\mu_2 \geq 0.285$. The equilibrium point is marginally stable because no damping is modeled between woodpecker and sleeve, but is stable in practice due to ever existing dissipation in reality.

Using the above data set, the motion of the woodpecker was simulated and a stable periodic solution was found with period time $T = 0.1452$ s. The time history of two periods of this periodic solution is shown in Figure 4 and the corresponding phase

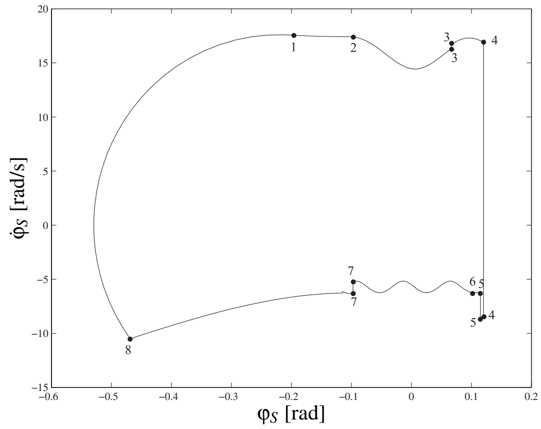

Figure 6. Phase space portraits.

space portraits in Figure 5 and 6. The numbers 1–8 correspond with the frames depicted in Figure 7. Let t_j denote the time at frame j. Just before $t = t_1$ the sleeve is jamming and the woodpecker is rotating upward, thereby reducing the normal force in contact 2. At $t = t_1$, the sleeve starts sliding downward, due to the reduced normal contact force, and contact is lost at $t = t_2$. In the time interval $t_2 < t < t_3$, the toy is in free fall and is quickly gaining kinetic energy. The first upper sleeve impact occur at $t = t_3$ but the contact immediately detaches. A beak impact occurs at $t = t_4$, which changes the direction of motion of the woodpecker. The beak impact is soon followed by the second upper sleeve impact at $t = t_5$. Detachment of the upper sleeve contact occurs at $t = t_6$. The toy is again in unconstrained motion during the time interval $t_6 < t < t_7$. A high frequency oscillation can be observed during this time interval and corresponds to the 72,91 Hz eigenfrequency of the woodpecker–spring–sleeve combination. Impact of the lower sleeve occurs at $t = t_7$, after which the sleeve is sliding down. The woodpecker is rotating downwards, increasing the normal force, and jamming of the sleeve starts at $t = t_8$. The succession of sliding and jamming of contact 2 transfers the kinetic energy of the translational motion in y direction , obtained during free falling, into rotational motion of the woodpecker. The woodpecker therefore swings backward when the lower sleeve contact jams, stores potential energy in the spring and swings forward again, $t = t_1 + T$, which completes the periodic motion.

Note that due to the completely filled mass matrix $\mathbf{M}$, an impact in one of the constraints affects each of the coordinates, which can be seen by the velocity jumps in the time histories and phase portraits of Figure 5 and 6.

The system has three degrees of freedom, which sets up a 6-dimensional state space $(\mathbf{q}, \dot{\mathbf{q}}) \in \mathbb{R}^6$. However, the accelerations $\ddot{\mathbf{q}}$ are only dependent on $\mathbf{z} = (\varphi_M, \varphi_S, \dot{\mathbf{q}}) \in \mathbb{R}^5$ and not on the vertical displacement y. The 6-dimensional system can therefore

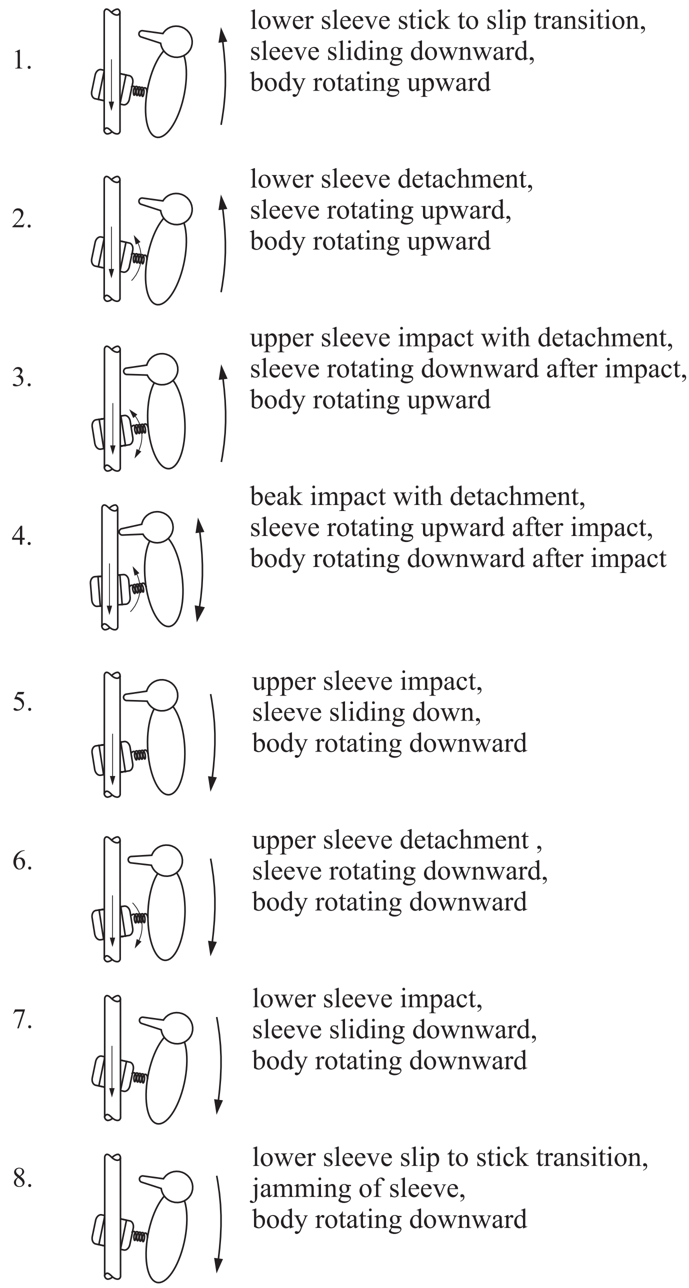

Figure 7. Sequence of events of the Woodpecker Toy.

be looked upon as a set of a 5-dimensional reduced system $\dot{\mathbf{z}} = \mathbf{f}(\mathbf{z})$ and a one-dimensional differential equation $\dot{y} = g(\mathbf{z})$. The on average deceasing displacement y can never be periodic. With a periodic solution of the system we mean periodic motion of the 5 states $\mathbf{z}$.

The reduced system $\mathbf{f}(\mathbf{z})$ possesses a set of solutions

$$\varphi_M = \varphi_S, |\varphi_M| \le (r_M - r_0)/h_M = 0.1034,$$
$$\dot{\varphi}_M = 0, \dot{\varphi}_S = 0, \dot{y} = gt + \dot{y}_0.$$

which correspond with a free falling motion of the toy along the shaft. This free falling can indeed be observed in the real toy, abruptly ended by an impact on the basement on which the shaft is mounted.

During the interval $t_8 < t < t_1 + T$, the sleeve is jamming and the woodpecker achieves a minimum rotation of $\varphi_S = -0.53$ rad. The rotation φ_S is the only non-constrained degree of freedom during jamming, which allows for a one-dimensional Poincaré mapping. Consider the 4-dimensional hyperplane Σ as a section of the 5-dimensional reduced phase space defined by

$$\Sigma = \{(\varphi_M, \varphi_S, \dot{\mathbf{q}}) \in \mathbb{R}^5 \mid \varphi_M = -(r_M - r_0)/h_M, \dot{\mathbf{q}} = \mathbf{0}\}. \quad (12)$$

If the woodpecker arrives at a local extremum for φ_S during jamming, then the state $\mathbf{z}$ must lie on Σ. From a state $\mathbf{z}_k \in \Sigma$, a solution evolves which may return to Σ at $\varphi_S = \varphi_{S_{k+1}}$. We define the one-dimensional first return map $P_1 : \Sigma \to \Sigma$ as

$$\varphi_{S_{k+1}} = P(\varphi_{S_k}). \quad (13)$$

Periodic solutions of period–1 and equilibria, which achieve a local extremum during jamming of the sleeve, are fixed points of P_1. Periodic solutions might exist, at least in theory, which do not contain a jamming part during the period (for instance when the friction coefficient μ_2 is small). Those types of solutions can not be found by means of this Poincaré map. Still, the map P_1 is suitable to study the manufacturers intended operation of the toy, which is a period–1 solution with jamming, and deviations from that.

The Poincaré map P_1 for $\varepsilon_{N1} = 0.5$ (being the restitution coefficient of the beak) is shown in Figure 8, obtained by numerical integration with 1000 initial values of φ_{S_k} (uniformly distributed between $-2.5 < \varphi_S < 0.11$ rad). The map appears to be very irregular and shows two distinct dips at $\varphi_S = -1.23$ rad and $\varphi_S = -0.27$ rad. These starting conditions lead to solutions evolving to the free falling motions along the shaft, and will consequently never return to the hyperplane Σ. Starting conditions around these singularities lead to solutions which fall for some time along the shaft, but finally return to constrained motion and to the section Σ. The kinetic energy, built up during the free fall, causes the woodpecker to swing tremendously backward, which explains the form of the dip: the smaller the return value $\varphi_{S_{k+1}}$, the longer the fall time was. The map has no value at the center of the dip, because the solution does not return to the Poincaré section. The dips are infinitely deep, but become smaller and steeper near the center. A finite depth is depicted due to the finite numerical accuracy. The most right dip consists of solutions which are directly trapped by the falling motion, whereas the left dip consists of solutions which first have an upper-sleeve impact before being trapped. More dips exist left of the depicted domain, all characterized by a sequence of events before the solution comes into free fall.

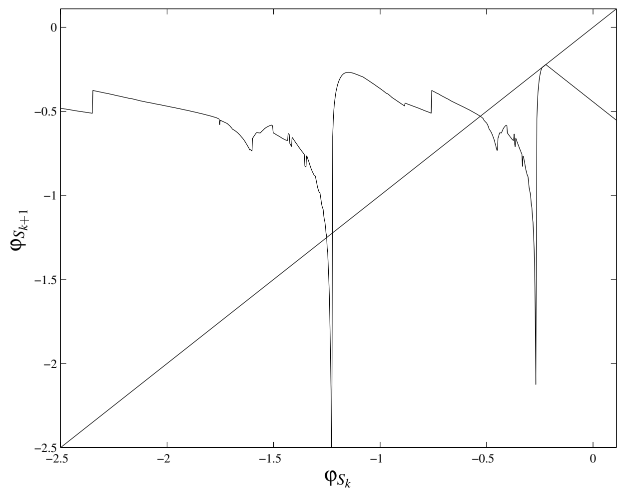

Figure 8. Poincaré map, $\varepsilon_{N1} = 0.5$.

Several points can be observed in Figure 8 on which the map is discontinuous (for instance at $\varphi_{S_k} = -0.76$ and -2.35 rad). The solution from a starting point on the section Σ undergoes several events (impacts, stick-slip transitions) before returning to Σ. The order, type and number of events in the sequence changes for varying initial conditions φ_{S_k}. When the order of two impact events changes at a critical initial condition φ_{S_c}, then a discontinuity in the solution occurs with respect to the initial condition. This discontinuity with respect to initial condition causes discontinuities in the Poincaré map. At the values $\varphi_{S_k} = -0.76$ and -2.35 rad for instance, the order of an upper sleeve impact and a beak impact are interchanged.

The Poincaré map P_1 has been calculated for 94 different values (not uniformly distributed) of the beak restitution coefficient ε_{N1} (where each mapping costs about one hour computation time). A bifurcation diagram was constructed from the set of mappings P by finding the crossings of the maps with the diagonal $\varphi_{S_{k+1}} = \varphi_{S_k}$. Each crossing is, for a locally smooth mapping, a stable or unstable periodic solution or equilibrium. The stability depends on the slope of the mapping at the crossing with the diagonal. The map P_1 is discontinuous and also the jumps in the map can have crossings with the diagonal. Those discontinuous crossings are, however, not periodic solutions or equilibria.

Figure 9 shows the period–1 solutions of the Woodpecker Toy for varying values of the restitution coefficient of the

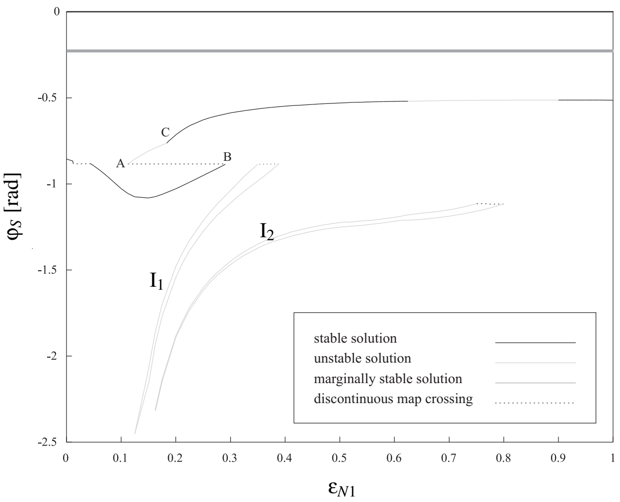

Figure 9. Bifurcation diagram, period–1 solutions.

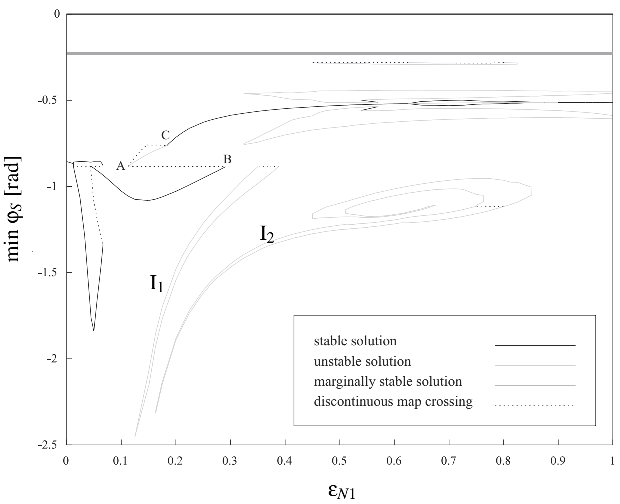

Figure 10. Bifurcation diagram, period–1 and 2 solutions.

beak ε_{N1}. Black lines indicate stable periodic solutions and light gray unstable periodic solutions. The woodpecker can oscillate with small amplitude around the equilibrium point. These solutions are centers, due to the lack of damping between sleeve and woodpecker, and are indicated by a dark gray band in Figure 9 around the equilibrium at $\varphi_S = -0.2216$. Discontinuous crossings of the map with the diagonal are indicated by dotted lines and connect stable and unstable branches of periodic solutions. Two stretched islands, I_1 and I_2, with unstable periodic solutions and discontinuous crossings can be observed in Figure 9. They are created by the two dips in the Poincaré map (Figure 8). It should be noted that the bifurcation diagram in Figure 9 is not

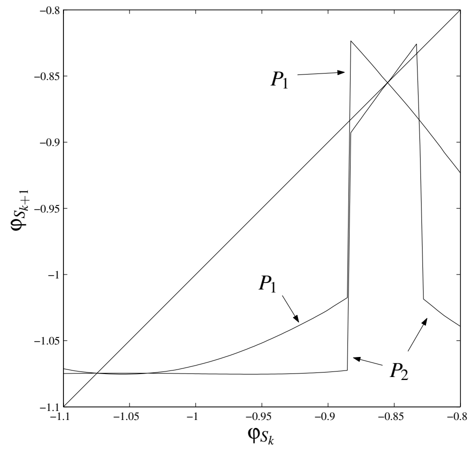

Figure 11. Zoom of the Poincaré maps for $\varepsilon_{N1} = 0.125$.

complete. Small islands and additional branches of periodic solutions/discontinuous crossings might have been lost by the finite accuracy and the finite domain of the P map. More islands probably exist due to additional dips left of the considered domain.

From the P_1 maps one can, in theory, construct higher order maps P_j, $j = 2, 3, ..$ by mapping P_1 onto itself, but the accuracy of the maps decrease for increasing order due to the finite discretization of P_1. The set of P_2 maps were constructed from the set of maps P_1. Figure 10 shows the period–2 solutions/discontinuous crossings (and also the period–1 solutions/crossings), obtained by finding the crossings of P_2 with the diagonal. Many additional branches appear in Figure 10, some branches of period–2 solutions, others discontinuous crossings of P_2 with the diagonal. Higher order branches (3 and higher) most surely also exist, but could not be computed accurately from P_1.

Branches of period–2 solutions appear in Figure 10 in pairs, as can be expected. It must hold for a period–2 solution that $\varphi_{S_{k+2}} = \varphi_{S_k}$ and $\varphi_{S_{k+3}} = \varphi_{S_{k+1}}$. In general holds that $\varphi_{S_{k+1}}$ is not equal to φ_{S_k} and they therefore appear as two different crossings in the P_2 map and as different branches in the bifurcation diagram. The two branches of one pair just contain the same periodic solution but shifted in time.

Very remarkable is that discontinuity crossings of P_2 do not appear in pairs, as can be seen for example at point A in Figure 10. At point A the branch of unstable period–1 solutions turns around and becomes a branch of P_1 discontinuity crossings, after which it is folded back to a stable branch at point B. A branch of P_2 discontinuity crossings bifurcates from the period–1 branch at A and makes a connection with point C. The P_2 discontinuity branch between A and C is clearly single (not a pair).

More insight into what exactly happens at the non-conventional bifurcation point A can be gained from a local analysis of the mappings P_1 and P_2. Figure 11 shows a zoom of P_1 and P_2 around the crossings of interest for $\varepsilon_{N1} = 0.125$, which is between A and C. The map P_1 is locally discontinuous and crosses the diagonal three times, leading to a stable and unstable solution and a discontinuity crossing. Studying the movement of the map for changing ε_{N1}, the map appeared to shift upward for increasing ε_{N1}. We will now study a simple piecewise linear discontinuous map, which locally approximates the numerically obtained P_1-map.

Consider the piecewise linear mapping, dependent on the constants $a > 1$ and r,

$$P_1^L(x) = \begin{cases} -2+r & x \leq 0 \\ -ax+r & x > 0 \end{cases} \tag{14}$$

which is depicted on the left in Figure 12 for $a = \frac{5}{4}$ and $r = 1$. The map shifts upward for increasing values of r. The map has two regular crossings with the diagonal

$$x = \frac{r}{1+a} > 0, \qquad x = -2+r < 0$$

for $r > 0$ and $r < 2$ respectively. A discontinuous crossing exists at $x = 0$ for $0 < r < 2$. Mapping $P_1^L(x)$ onto itself gives $P_2^L(x)$:

$$P_2^L(x) = \begin{cases} -2+r & x \leq 0 \\ a^2x+(1-a)r & 0 < x < \frac{r}{a} \\ -2+r & x \geq 0 \end{cases} \tag{15}$$

and is depicted in the right picture of Figure 12. The $P_2^L(x)$ map is again piecewise linear in x and has two discontinuities at $x = 0$ and $x = \frac{r}{a}$. The same regular crossings of P^L appear of course in P_2^L. Additionally, $P_2^L(x)$ has a *single* discontinuous crossing with the diagonal at $x = \frac{r}{a}$ but does not contain a discontinuous crossing at $x = 0$, like P_1^L. Note that P_1^L and P_2^L look indeed similar to P_1 and P_2 in Figure 11. Varying r gives the bifurcation diagram depicted in the right of Figure 12, which is similar to what can be observed in Figure 10 around point A. Point B is also retrieved from the piecewise linear analysis. The local analysis by the piecewise linear map only predicts the behaviour in a small neighbourhood of point A. The bifurcation at point C is due to other changes in the map P_1 and can therefore not be observed in Figure 12.

Remark that regular crossings of P^L are also regular crossings of P_2^L, because they correspond to the periodic solutions and equilibria of the system. Discontinuous crossings of P^L are in general *not* discontinuous crossings of P_2^L.

Branches of higher order discontinuous crossings of P_j^L, $j > 2$, also start at point A. It can therefore be expected that these branches can also be found for the Woodpecker Toy if the higher order maps would be calculated accurately.

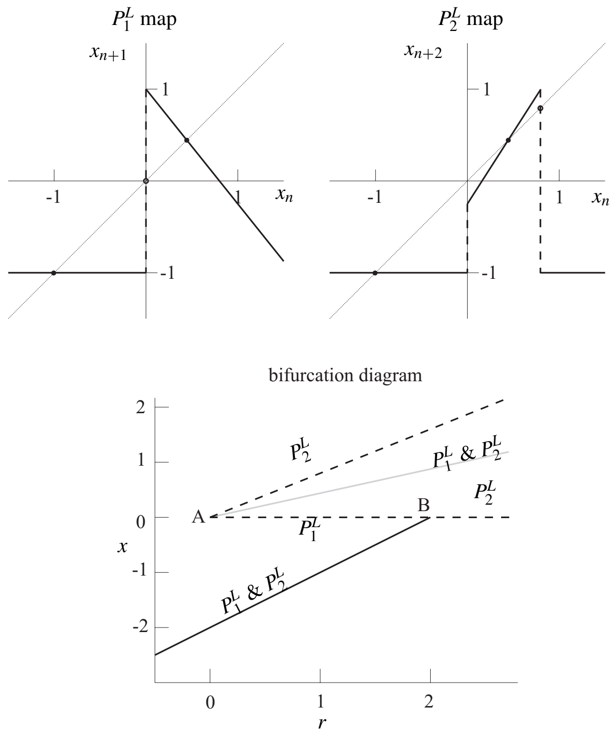

Figure 12. Analytical analysis of point A in Figure 10.

Bifurcation point A shows behaviour similar to a fold bifurcation, at which a branch is folded around, albeit that the branch changes to a branch of discontinuous crossings after folding. Apart from the folding action, also a branch with P_2 discontinuous crossings bifurcate from the period–1 branch. In some sense, this behaviour is similar to a flip or period-doubling bifurcation, at which a period-doubled solution bifurcates from the period–1 branch. The bifurcation point A therefore shows both folding and a kind of flip action. This is not in conformity with the bifurcation theory for smooth systems, which predicts that bifurcations are either fold or flip bifurcations (or of other type). Bifurcation point A is therefore a non-conventional bifurcation point. A similar bifurcation point, showing both fold and flip action, was found for a system of Filippov-type in [Leine *et al.*, 2000, Leine, 2000]. The combined fold–flip behaviour is related to the tent map, which is more elaborately explained in [Leine *et al.*, 2000, Leine, 2000]. Remark that the P_1 map shows indeed a peak, similar to the tent map, although one flange is vertical.

CONCLUSIONS

The nonlinear dynamics of the Woodpecker Toy was studied in this paper. The analysis is not complete, because many other parameters can be varied. The chaotic attractors are also not considered. Still, the variation of ε_{N1} gives more insight in the complex dynamical phenomena present in the system. A one-dimensional mapping was found for the Woodpecker Toy. This mapping turns out to be very valuable for the construction of bifurcation diagrams, because it detects not only the periodic solutions but also the discontinuity crossings. Branches of discontinuity crossings appear to connect branches of periodic solutions and are therefore a new kind of objects in the bifurcation diagram, different from attractors. Furthermore, the one-dimensional mapping can be used to gain a better understanding of non-conventional bifurcation points.

REFERENCES

Beitelschmidt, M. (1999). *Reibstöße in Mehrkörpersystemen*, Fortschr.-Ber. VDI Reihe 11, Nr. 275, VDI Verlag, Düsseldorf.

Blazejczyk-Okolewska, B. and Kapitaniak, T.(1996). 'Dynamics of Impact Oscillator with Dry Friction', *Chaos, Solitons & Fractals*, **7**(9), pp. 1455-1459.

Brogliato, B. (1999). *Nonsmooth Mechanics*, Springer, London.

Cottle, R. W. and Dantzig, G. B. (1968). 'Complementary pivot theory of mathematical programming', *Linear Algebra and its Applications*, **1**, pp. 103-125.

Dankowicz, H. and Nordmark, A. B. (2000). 'On the origin and bifurcations of stick-slip oscillations', *Physica D*, **136**(3-4), pp. 280-302.

di Bernardo, M., Feigin, M. I., Hogan, S. J. and Homer, M. E. (1999). 'Local analysis of C-bifurcations in n-dimensional piecewise-smooth dynamical systems', *Chaos, Solitons & Fractals*, **10**(11), pp. 1881-1908.

Foale, S. and Bishop, R. (1994). 'Bifurcations in Impacting Oscillations', *Nonlinear Dynamics*, **6**, pp. 285-299.

Galvanetto, U., and Knudsen, C. (1997). 'Event Maps in a Stick-slip System', *Nonlinear Dynamics*, **13**(2), pp. 99-115.

Glocker, Ch. (1995). *Dynamik von Starrkörpersystemen mit Reibung und Stößen*, Fortschr.-Ber. VDI Reihe 18, Nr. 182, VDI Verlag, Düsseldorf.

Glocker, Ch. (2000), 'Scalar force potentials in rigid multibody systems' in *Multibody Dynamics with Unilateral Contacts* (eds. F. Pfeiffer, Ch. Glocker), CISM Courses and Lectures Vol 421, Springer, Wien 2000, pp. 69-146.

Guckenheimer, J. and Holmes, P. (1983). *Nonlinear Oscillations, Dynamical Systems, and Bifurcations of Vector Fields*, Applied Mathematical Sciences 42, Springer-Verlag, New York.

Ivanov, A. P. (1996). 'Bifurcations in Impact Systems', *Chaos, Solitons & Fractals*, **7**, 10, pp. 1615-1634.

Leine, R. I. and Van Campen, D. H. (1999). 'Fold Bifurcations in Discontinuous Systems', *Proceedings of DETC'99 ASME Design Engineering Technical Conferences*, September 12-15, Las Vegas, CD-ROM, DETC99/VIB-8034.

Leine, R. I. and Van Campen, D. H. (2000). 'Discontinuous Bifurcations of Periodic Solutions', accepted for publication in *Mathematical Modelling of Nonlinear Systems*.

Leine, R. I., Van Campen, D. H. and Van de Vrande, B. L. (2000). 'Bifurcations in Nonlinear Discontinuous Systems', *Nonlinear Dynamics*, **23**(2), pp. 105-164.

Leine, R.I. (2000). *Bifurcations in Discontinuous Mechanical Systems of Filippov-Type*. Ph.D. thesis, Eindhoven University of Technology, The Netherlands.

Meijaard, J. P. (1996). 'A mechanism for the onset of chaos in mechanical systems with motion-limiting stops', *Chaos, Solitons & Fractals*, **7**(10), pp. 1649-1658.

Nordmark, A. B. (1997). 'Universal limit mapping in grazing bifurcations' *Physical review E*, **55**(1), pp. 266-270.

Peterka, F. (1996). 'Bifurcations and Transition Phenomena in an Impact Oscillator', *Chaos, Solitons & Fractals*, **7**(10), pp. 1635-1647.

Pfeiffer, F. (1984). 'Mechanische Systeme mith unstetigen Übergängen', *Ingenieur-Archiv*, **54**, pp. 232-240.

Pfeiffer, F. and Glocker, Ch. (1996). *Multibody dynamics with unilateral contacts*, Wiley, New York.

Popp, K., Hinrichs, N. and Oestreich, M. (1995). 'Dynamical behaviour of a friction oscillator with simultaneous self and external excitation', in *Sādhānā: Academy Proceedings in Engineering Sciences*, Indian Academy of Sciences, Banglore, India, Part 2-4, **20**, pp. 627-654.

Van de Vrande, B. L., Van Campen, D. H. and De Kraker, A. (1999). 'An Approximate Analysis of Dry-Friction-Induced Stick-slip Vibrations by a Smoothing Procedure', *Nonlinear Dynamics*, **19**(2), pp. 157-169.

Wiercigroch, M. (1996). 'On Modelling Discontinuities in Dynamic Systems', *Machine Vibration*, **5**, pp. 112-119.

Yoshitake, Y. and Sueoka, A. (2000). 'Forced Self-exited Vibration Accompanied by Dry friction', in: 'Applied Nonlinear Dynamics and Chaos of Mechanical Systems with Discontinuities', M. Wiercigroch and A. de Kraker (eds.), World Scientific.